Applied Clay Science 141 (2017) 257–264

Contents lists available at ScienceDirect

Applied Clay Science

journal homepage: www.elsevier.com/locate/clay

Research paper

Risedronate functionalized layered double hydroxides nanoparticles with bone targeting capabilities

Dariana Aristizabal Bedoya, Cecilia Vasti, Ricardo Rojas, Carla E. Giacomelli *

INFIQC-CONICET, Departamento de Fisicoquímica, Facultad de Ciencias Químicas, Universidad Nacional de Córdoba, Ciudad Universitaria, 5000 Córdoba, Argentina

ARTICLE INFO

Article history:
Received 24 January 2017
Received in revised form 28 February 2017
Accepted 1 March 2017
Available online xxxx

Keywords:
Nanocarriers
pH responsive
Hydroxyapatite binding
Colloidal stability
Bisphosphonates

ABSTRACT

Layered double hydroxides nanoparticles (LDH-NPs) are increasingly studied as drug nanocarriers for cellular delivery. Nevertheless, stable functionalizations providing targeting capabilities without disrupting the size of the carriers are necessary to achieve optimized performance. Here, LDH-NPs were functionalized with risedronate (Ris) to improve the osteotropicity of the nanocarriers without altering the nanosized distribution. Ris is a nitrogen containing bisphosphonate with rich acid-base reactivity that can lead Ris functionalized LDH-NPs also as pH-responsive drug nanocarriers. The current work is focused on the strategy to synthesize functionalized LDH-NPs with a maximum adsorption and a minimum intercalation of Ris while maintaining their nanosize. The speciation and interactions of Ris at the surface of LDH-NPs were analyzed using Raman microscopy whereas the functionalization stability and size distribution were checked in simulated biological media. Finally, pH sensitivity and hydroxyapatite binding capacity of Ris functionalized LDH-NPs were evaluated. $HRis^{3-}$ anions were incorporated to the LDH-NPs surface with high affinity providing with a negative zeta potential that controlled the size at around 100 nm. The size of Ris functionalized LDH-NPs was not affected by the high ionic strength or the presence of proteins in simulated biological media. Further, the functionalization was stable against protein adsorption and anionic exchange. As expected, Ris functionalized LDH-NPs are bioresponsive with a high sensitivity for pH changes and specific affinity for hydroxyapatite, which makes them appealing drug nanocarriers for new bone therapies.

1. Introduction

Both bone targeting and efficient cellular internalization of drugs are two challenges for treating musculoskeletal diseases such as osteoporosis or bone cancer. Many novel pharmaceutical agents have been designed but most of them present low to negligible specific distribution to hard tissues, which results in toxicity (Wang et al., 2005; LeVasseur et al., 2016). Nanotechnology has created a great opportunity in more efficient and safer bone nanotherapies, able to produce targeted delivery of drugs and biomolecules (Conde et al., 2014). Layered double hydroxides nanoparticles (LDH-NPs) are excellent matrixes to be used as drug nanocarriers due to their low cost and easy synthesis and modification, high loading capacity and good biocompatibility (Rives et al., 2014; Kuthati et al., 2015; Saha et al., 2017). LDH-NPs present stacks of brucite ($Mg(OH)_2$)-like layers that are positively charged as a result of the isomorphic substitution by Al^{3+} ions. They are synthesized by methods that involve separate precipitation and aging steps (Xu et al., 2006; Ladewig et al., 2010; Chung et al., 2012; Chen et al., 2013). Drugs, such as non-steroidal anti-inflammatories, anticancer drugs, antibiotics and biomolecules (proteins, DNA, siRNA, etc.) have been incorporated to their structure (Costantino et al., 2009; Conterosito et al., 2013; Rodrigues et al., 2013; Ma et al., 2014). LDH-NPs are able to interact with cellular membrane and they exhibit enhanced cellular internalization by a clathrin pathway (Oh et al., 2006; Wong et al., 2010; Choi and Choy, 2011). Once internalized, LDH-NPs present a drug release mechanism related to its solubility in acid media, activated by the increasingly acid media in endosomes (Medina-Kauwe et al., 2005; Chung et al., 2012).

Nevertheless, functionalization of LDH-NPs is necessary to provide features such as colloidal stability in biological media, drug release modification and targeting ability, essential to their performance as drug nanocarriers (Hu et al., 2013; Wang et al., 2014; Kuo et al., 2015; Ray et al., 2015). Thus, functionalization with albumin (Gu et al., 2015; Zuo et al., 2015) and polyethylene glycol chains (Li et al., 2011; Zhang et al., 2014) has been reported to improve colloidal stability of LDHNPs. Moreover, functionalization with folic acid has been proposed to increase the internalization of LDH-NPs by tumor cells with overexpression of folate receptors (Oh et al., 2009).

Surface functionalization of LDH-NPs with bisphosphonates (BPs) is expected to provide them with bone targeting capability (osteotropicity). BPs have P-C-P groups where the central carbon

* Corresponding author.
E-mail address: giacomel@fcq.unc.edu.ar (C.E. Giacomelli).

http://dx.doi.org/10.1016/j.clay.2017.03.001
0169-1317/

can be modified with different substituents, which lead to a large family of compounds. They were first applied as antiresorptive agents due to the analogy of P-C-P groups to pyrophosphate, which lead to a high affinity for bone hydroxyapatite. BPs have been also reported to treat bone metastasis and multiple myeloma (Coleman and McCloskey, 2011). Due to their affinity for bone apatites, much effort has been devoted to conjugate them with specific therapeutic agents to produce osteotropicity (Wang et al., 2005). This strategy has been extended to polymeric (Ramanlal Chaudhari et al., 2012) calcium phosphate or metal oxide NPs (Ossipov, 2015) to prepare drug nanocarriers suitable for systemic bone treatment. Although LDHs have been intercalated with BPs, such as alendronate (Nakayama et al., 2003) and etidronic acid (Chakraborti et al., 2011), and the drug release from the synthesized hybrids has been explored, BPs surface functionalization of LDHs has not been proposed.

The objective of this work is to functionalize the surface LDH-NPs with risedronate (Ris) to improve the osteotropicity of the nanocarriers without altering the nanosized distribution. Ris is a third generation, nitrogen containing BPs with a much higher potency than alendronate and etidronic acid (Meloun et al., 2012). Moreover, the presence of a pyridine group in its structure leads to a rich acid-base reactivity in the 5–7 pH range, which is expected to induce pH sensitivity to LDH-NPs. pH-responsive drug nanocarriers are used to produce passive targeting of tumoral tissues (Lee et al., 2008; Zhu et al., 2016; Kankala et al., 2017) due to the pH changes in the microenvironment of tumors. Therefore, Ris functionalization may provide LDH-NPs with targeting capabilities in bone tumoral tissues. The current work is focused on the synthesis strategy in order to synthesize functionalized LDH-NPs with a maximum adsorption and a minimum intercalation of Ris while maintaining their nanosize. The speciation and interactions of Ris at the surface of LDH-NPs were analyzed using Raman microscopy and the functionalization stability was checked in two different media that were intended to reproduce the pH of blood plasma and the slightly acidic environment of cell organelles, such as lysosomes (Wang et al., 2011). On the other hand, the size distribution of the Ris functionalized LDH-NPs was evaluated in three relevant biological media: physiological and Ringer solutions and simulated plasma. Finally, pH sensitivity and hydroxyapatite binding capacity of Ris functionalized LDH-NPs were evaluated as a first step towards the optimization of the bioresponsive properties of LDH-NPs based nanocarriers.

2. Materials and methods

Reagent grade $MgCl_2 \cdot 6H_2O$, NaOH, $NaHCO_3$werepurchased from Cicarelli; $AlCl_3 \cdot 6H_2O$, KCl, $CaCl_2$, from Anedra; NaCl, K_2HPO4, KH_2PO4 from J.T. Baker; bovine serum albumin (Alb) from Sigma-Aldrich, while sodium risedronate hemipentahydrate (Ris) was gently provided by IVAX, Argentina. The reagents were used with no previous purification. All solutions were prepared with purified water (18 MΩ Milli Q, Millipore System) and all experiments, unless otherwise stated, were performed at room temperature.

2.1. Ris functionalized LDH-NPs

As a first step, chloride intercalated Mg-Al-LDH nanoparticles (bare LDH-NPs) were synthesized by a coprecipitation method at constant pH involving separate nucleation and aging steps (Vasti et al., 2016). A 100 mL solution containing 0.06 mol $MgCl_2$ and 0.02 mol $AlCl_3$ was added dropwise to a 200 mL solution containing 0.02 mol NaCl. The pH of the media was set to 9 by addition of a 2 mol L^{-1} NaOH solution. Once the addition was finished, the prepared solid was separated by centrifugation and washed twice with water. Subsequently, a 500 mL dispersion of the solid was prepared, and afterwards submitted to hydrothermal treatment at 80 °C for 16 h. A portion of the resulting dispersion was freeze-dried to perform the chemical and structural characterization of the sample.

In a second step, Ris functionalized LDH-NPs were prepared by adsorbing the drug at conditions that led to a complete surface coverage by the anions, low intercalation between the layers and the size in the nanometer range With such a purpose, the functionalization of LDH-NPs was studied in dispersions (1.00 g L^{-1} LDH-NPs) with increasing Ris concentration ([Ris] ranging from 0.07 to 5.9 mmol L^{-1}) equilibrated overnight, the final pH being between 8.5 and 9.5 in all cases. To determine the sorbed amount of Ris (Γ_{Ris}, g g^{-1}), the concentration in the supernatants was measured by UV–vis spectrophotometry (Shimadzu UV1601, Japan) at $\lambda = 262$ nm. The optimum condition was found to be 0.1 L Ris solution (0.021 mol L^{-1}, pH = 9) added to a 1 L LDH-NPs dispersion (5.7 g L^{-1}) and equilibrated overnight.

Bare and Ris functionalized LDH-NPs were characterized in order to determine their composition, morphology and structural features. Mg and Al contents were measured by atomic absorption spectrometry in a Varian AA240 instrument. The samples were dissolved in HNO_3 and afterwards diluted to meet the calibration range. C and N content was determined in a CHN 2400 Serie II Elemental Analyzer, using cysteine as reference. Water content was determined by thermogravimetric and differential thermal analyses (TG/DTA), which were performed in a Shimadzu DTG 60 instrument, in flowing air at a heating rate of 10 °C min^{-1}. Powder X-ray diffraction (PXRD) patterns were recorded in a Phillips X'pert Pro instrument using a Cu Kα lamp ($\lambda = 1.5408$ Å) at 40 kV and 40 mA in step mode (0.05°, 1.2 s). FT-IR spectra were measured in a Bruker IFS28 instrument using KBr pellets (1:100 sample:KBr ratio). Raman spectra were measured in a Raman confocal microscope LABRAM-HR, Horiba Jobin-Yvon. Scanning electron microscopy (SEM) images were obtained in a FE-SEM Σigma instrument on samples covered with a Cr layer. The samples were prepared from LDH-NPs dispersions, which were diluted 1:100 in ethanol. A drop of a 0.1 g L^{-1} dispersion was placed on the aluminum holder and dried at 60 °C.

2.2. Size of Ris functionalized LDH-NPs in media of biological relevance

The size of bare and Ris functionalized LDH-NPs was evaluated in different media of biological relevance. Hydrodynamic apparent diameter (d) and zeta potential (ζ) values were determined by dynamic light scattering (DLS) and electrophoretic light scattering (ELS) measurements using a Delsa Nano C instrument (Beckman Coulter). d and ζ measurements were performed on 1 g L^{-1} dispersions in physiological (NaCl 150 mmol L^{-1}) and Ringer solutions (NaCl 110 mmol L^{-1}; KCl 5,6 mmol L^{-1}; $CaCl_2$ 2,25 mmol L^{-1}; $NaHCO_3$ 2,4 mmol L^{-1}) and simulated plasma (Ringer solution, supplemented with 40 g L^{-1} albumin).

The effect of relevant parameters of the biological media (ionic strength and protein concentration) on the size of both samples was also evaluated in 1 g L^{-1} dispersions as a function of NaCl ([NaCl] ranging from 0 to 0.25 mol L^{-1}) or albumin ([Alb] ranging from 0 to 0.55 g L^{-1}) concentrations.

2.3. Stability of Ris functionalized LDH-NPs in media of biological relevance

To test the stability of the functionalization in relevant biological conditions, desorption kinetics was studied on Ris functionalized LDH-NPs (1 g L^{-1}) dispersed in phosphate (PB, pH = 7.4) and acetate (AB, pH = 4.7 ± 0.1) buffer solutions. The first medium was intended to reproduce the pH of blood plasma in the presence of phosphate, an anion with a high affinity for LDHs (Rojas et al., 2012). On the contrary, AB presents a slightly acidic pH that has been associated to that of acidic cell organelles such as lysosomes (Wang et al., 2011). Ris desorption (%Ris) was determined by the percentage between the concentration of Ris in the supernatants and the amount of Ris initially adsorbed.

2.4. pH response of Ris functionalized LDH-NPs

The proton uptake (Γ_H) as a function of the pH was used to evaluate the pH responsive behavior of bare and Ris functionalized LDH-NPs. The experiments were conducted in separate 1 g L^{-1} dispersions with increasing acid chloride concentration ([HCl]). These dispersions were equilibrated overnight and, finally, %Ris, ζ and d values were measured as previously described.

2.5. Hydroxyapatite binding capacity of Ris functionalized LDH-NPs

The binding capacity towards Ca^{2+} ions, either in solution or as part of hydroxyapatite (Hap), was studied as a first indication of the osteotropic capacity of bare and Ris functionalized LDH-NPs. In the first case, dispersions (1 g L^{-1}, 5 mmol L^{-1} NaCl) with increasing Ca^{2+} concentration ([$CaCl_2$] up to 3 mM) at pH = 9 were prepared. These dispersions were equilibrated overnight, and then %Ris, d and ζ values were determined as previously described. The affinity of LDH-NPs for Hap was explored by streaming potential determinations in a SurPASS 3 electrokinetic analyzer (Anton Parr). Hap powder was sandwiched between two membranes and its ζ was measured in 0.5 M KCl solution. Then, dispersions (1 g L^{-1}) of bare and functionalized LDH-NPs in the same media were passed through the Hap sample. As a complement, SEM images were measured with Hap disks soaked in dispersions (1 g L^{-1}) of bare and functionalized LDH-NPs. The Hap disks were prepared by compression at 2 tons in an 11 mm die, and they were soaked for 10 s in the corresponding dispersion and finally washed with water carefully.

3. Results and discussion

3.1. Ris functionalized LDH-NPs

In order to determine the optimum conditions for LDH-NPs functionalization, Ris uptake (Γ_{Ris}) was studied as a function of Ris concentration ($[Ris]_{eq}$) (Fig. 1A). The figure shows three different regimes: an initial steep slope at $[Ris]_{eq}$ near 0 that flattened (Γ_{Ris} = 0.3 mmol g^{-1}) before reaching the final plateau at Γ_{Ris} = 0.6 mmol g^{-1}. Increasing Γ_{Ris} values produced changes in both d and ζ values (Fig. 1B). A continuous ζ decrease from 40 to −40 mV was registered up to Γ_{Ris} = 0.3 mmol g^{-1}, whereas d increased from 100 nm (bare LDH-NPs) to a few μm at Γ_{Ris} < 0.3 mmol g^{-1} and decreased again to the initial value at higher Γ_{Ris}. Finally, the PXRD patterns (Fig. 1C) showed well defined *(00l)* peaks with similar intensity up to Γ_{Ris} around 0.3 mmol g^{-1} while the peaks intensity decreased as Γ_{Ris} increased at higher values. The steeply initial increase of Γ_{Ris}, indicated that Ris anions incorporated with high affinity to the surface of LDH-NPs, which is in line with the ζ reversal, the size change as well as the features in the PXRD patterns observed up to Γ_{Ris} around 0.3 mmol g^{-1}.

Risedronic acid (H_5Ris^+) dissociates releasing up to 5 protons as pH increases (Fig. 2A), their pK_a values being 1.6, 2.8, 5.3, 6.7 and 10.5 (Meloun et al., 2012; Errassifi et al., 2014). The Raman spectra of both NaH_3Ris and Na_3HRis (Fig. 2B) showed characteristic bands of the phosphonate groups in the 850–1000 cm^{-1} and 1150–1250 cm^{-1} range. The main differences were found in the 1000–1100 cm^{-1} range, where the characteristic bands of the pyridine group are located (Redman-Furey et al., 2005; Errassifi et al., 2014). NaH_3Ris showed two intense bands at 1057 and 1028 cm^{-1}, the former being more intense than the latter. On the other handNa_3HRis showed bands at 1054 and 1039 cm^{-1} and, contrarily to that determined for NaH_3Ris, the band at larger wavenumbers was more intense that the one at the lower wavenumber. The spectral features of Ris functionalized LDH-NPs were similar to those of NaH_3Ris, indicating the uptake of $HRis^{3-}$ which was the most likely anion to be incorporated due to the pH conditions during the functionalization experiments.

The three negative charges of $HRis^{3-}$ as well as the different groups capable of establishing hydrogen bonding with the LDH-NPs layers are responsible for the high affinity of Ris. Our results indicated that $HRis^{3-}$ anions were first incorporated to the LDH-NPs surface causing the ζ inversion without modifying the PXRD pattern. When the particle

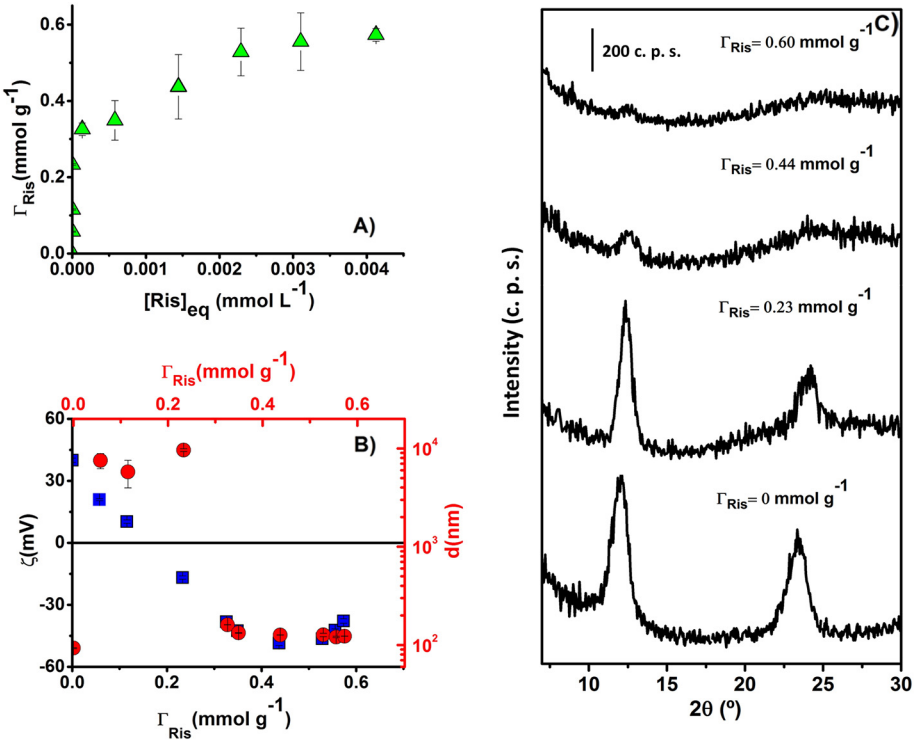

Fig. 1. A) Risedronate (Ris) uptake (Γ_{Ris}) of LDH-NPs as a function of the Ris concentration in steady state conditions ($[Ris]_{eq}$), B) on the left axis, zeta potential (ζ, squares) and, on the right axis, hydrodynamic apparent diameter (d, circles) as a function of Γ_{Ris}, C) PXRD patterns of samples at different Γ_{Ris}. Error bars represent the standard deviation, calculated from 3 experimental runs.

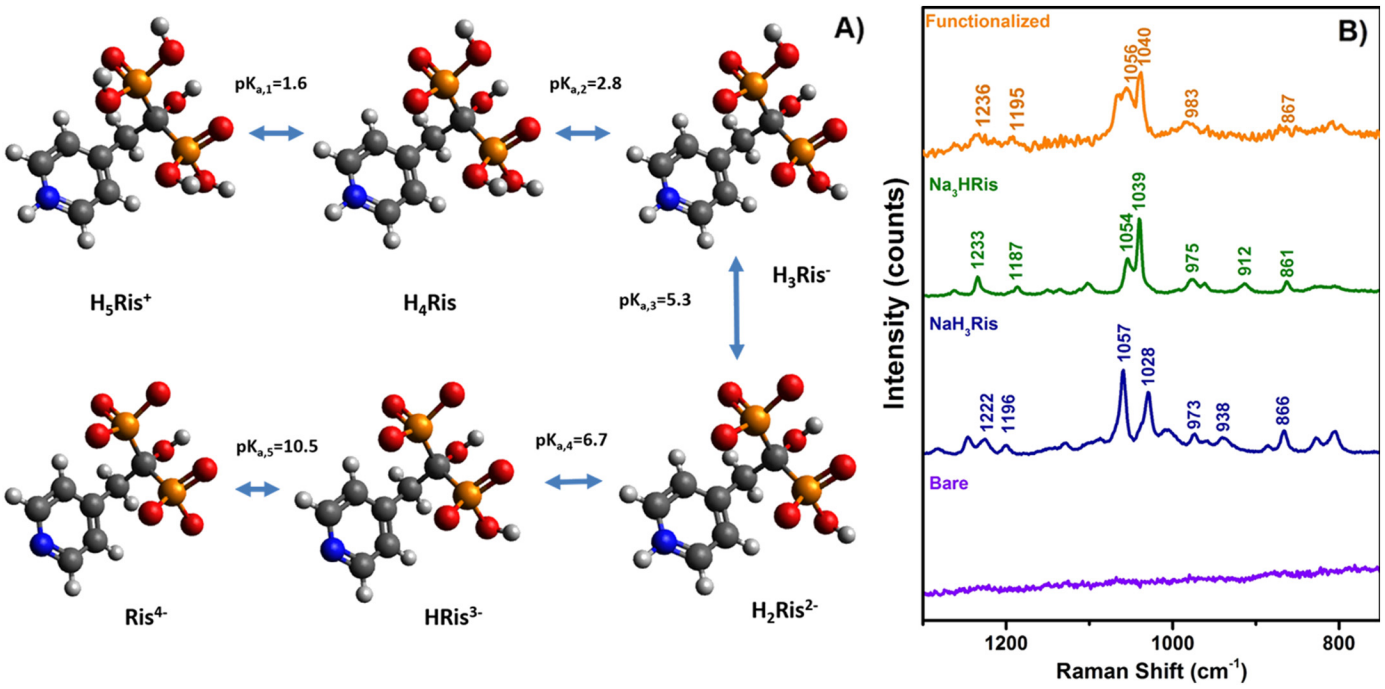

Fig. 2. A) Chemical structures and acid base-equilibria of risedronate (Ris), B) Raman spectra of NaH_3Ris andNa_3HRis salts as well as bare and functionalized LDH-NPs.

is positively charged, these anions are interacting with the surface with both phosphonate groups but, when the particle becomes negatively charged, it can be expected that a portion of $HRis^{3-}$ anions interacted with only one group, and the other one faced to the aqueous side of the interface. Due to the adsorption of the $HRis^{3+}$ anions, the electrostatic repulsions increased at the surface and the intercalation between the layers of LDH-NPs became favorable. Consequently, the slope of Γ_{Ris} vs. $[Ris]_{eq}$ decreased and no further changes in ζ values were produced. $HRis^{3-}$ intercalation was also evident from the intensity decrease of (*00l*) peaks in the PXRD patterns at $\Gamma_{Ris} > 0.3$ mmol g^{-1}.

Based on these experiments, Ris functionalized LDH-NPs were prepared with *d* values around 100 nm, maximum surface functionalization and minimum intercalation ($\Gamma_{Ris} = 0.4$ mmol g^{-1}). Chemical analysis data, PXRD patterns and SEM images of bare and functionalized LDH-NPs are included as Supporting Information (Table S1 and Figs. S1 and S2). Based on the chemical composition, we verified that a high surface functionalization without affecting the composition of the interlayer, <40% of the exchange sites (including those at the surface of the particles) being occupied by $RisH^{3-}$ anions. At the same time, the SEM images confirmed that the functionalization of LDH-NPs did not affect their characteristic lamellar morphology with hexagonal symmetry.

3.2. Size of Ris functionalized LDH-NPs in media of biological relevance

Size is one of the main features that affects the performance of drug nanocarriers; biological media are expected to induce some degree of aggregation due to their high ionic strength and complex composition. *d* values of bare and Ris functionalized LDH-NPs were tested in simulated biological media, such as physiological and Ringer solutions and simulated plasma (Fig. 3). Although both solutions are isotonic respect to the biological media, physiological solution contains only NaCl while Ringer solution includes the three major metal ions in the biological media (Na^+, K^+ and Ca^{2+}). Finally, simulated plasma differs with Ringers solution in the inclusion of albumin at a concentration similar to that of human plasma (40 g L^{-1}). The size of functionalized LDH-NPs, contrarily to that of the bare ones, was not affected by the high ionic strength of physiological solution. To understand the improved colloidal stability of Ris functionalized LDH-NPs compared to the bare ones, the dependence of *d* and ζ with the ionic strength was studied in dispersions with increasing NaCl concentration ([NaCl]) (supporting information, Fig. S3). Ris functionalized LDH-NPs only increased their *d* values to 300 nm when [NaCl] = 0.25 mol L^{-1}, while bare LDH-NPs aggregated to several μm at [NaCl] < 0.10 mol L^{-1}. On the contrary, *d* values greatly increased in Ringer solution for both samples, which was due to the diminution of the ζ values. Both effects are determined by the interaction of $HRis^{3-}$ anions with Ca^{2+} ions, which will be fully discussed below (Section 3.4).

Finally, the presence of albumin kept the nanosized distribution of both bare and Ris functionalized LDH-NPs despite the low, negative ζ values. Hence, the effect of the protein concentration on bare and functionalized LDH-NPs was also analyzed (supporting information, Fig. S5)

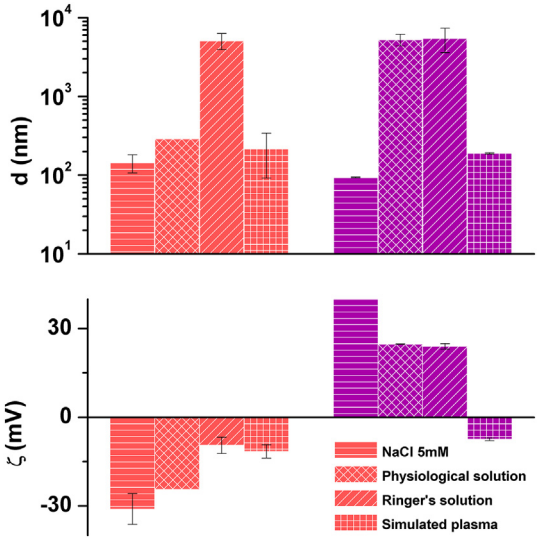

Fig. 3. Hydrodynamic apparent diameter (*d*) and zeta potential (ζ) of bare and Ris functionalized LDH-NPs (1 g L^{-1}) in relevant biological media (physiological and Ringer solutions and simulated plasma). Error bars represent the standard deviation, calculated from 3 experimental runs.

by adsorption isotherms in physiological solution. The positively charged bare LDH-NPs presented high affinity for the negatively charged albumin (iep 4.73 (Vermonden et al., 2002)), leading to a high maximum adsorbed amount ($\Gamma_{max} = 1.65$ g g^{-1}). Contrarily, the low Γ_{max} value ($=0.20$ g g^{-1}) on Ris functionalized LDH-NPs was due to the repulsive electrostatic interactions nanoparticles-protein as well as the high affinity of $HRis^{3-}$ for the surface of LDH-NPs that was not displaced by albumin. Increasing surface coverage (Γ/Γ_{max}) produced only a slight ζ increase for Ris functionalized LDH-NPs, while a charge reversal from positive to negative for bare LDH-NPs. As a consequence, both samples presented converging ζ values at $\Gamma/\Gamma_{max} = 1$, which indicated that ζ were determined by the protein corona, similarly to that found for other LDH-NPs and metal oxides (Tantra et al., 2010; Vasti et al., 2016). On the other hand, the d dependence with Γ/Γ_{max} was similar for both samples: d values increased at low Γ/Γ_{max} and decreased at high Γ/Γ_{max}, reaching 100–200 nm at $\Gamma/\Gamma_{max} = 1$. Therefore, the formation of the protein corona ($\Gamma/\Gamma_{max} = 1$ and simulated plasma) inhibited the aggregates formation of both bare and Ris functionalized LDH-NPs. This colloidal stability was not due to electrostatic interactions, as the converging ζ values were lower than those at $\Gamma/\Gamma_{max} = 0$, but steric hindrance was responsible for the size measured in simulated plasma.

3.3. Stability of Ris functionalized LDH-NPs in media of biological relevance

To test the stability of the functionalized LDH-NPs against Ris desorption in significant biological pH conditions, desorption (%Ris) kinetics in PB (intended to reproduce the pH of blood plasma) and AB (associated to the acidic cell organelles), were also measured (Fig. 4). The interaction between Ris and LDH-NPs is so strong that even in the presence of phosphate, an anion with a high affinity for LDHs (Rojas et al., 2012), the desorption was low (<10%) at any given time. Hence, the functionalization would be highly stable in blood plasma. On the contrary, the functionalization was completely removed after 1 h in acid media. This effect may be due to the protonation of $HRis^{3-}$ that gives less charged anions with lower affinity for LDH-NPs or to the nanoparticles dissolution. In any case, the functionalization of LDH-NPs would be lost in the acidic cell organelles once the nanoparticles were internalized by cells. It is also worth mentioning that Ris desorption was low (<20%) even at [NaCl] = 0.25 mol L^{-1} (Supporting information, Fig. S3), much higher than isotonic solutions respect to the biological media (0.15 mol L^{-1}). Generally speaking, the functionalization is highly stable in biological relevant conditions for the parenteral drug delivery.

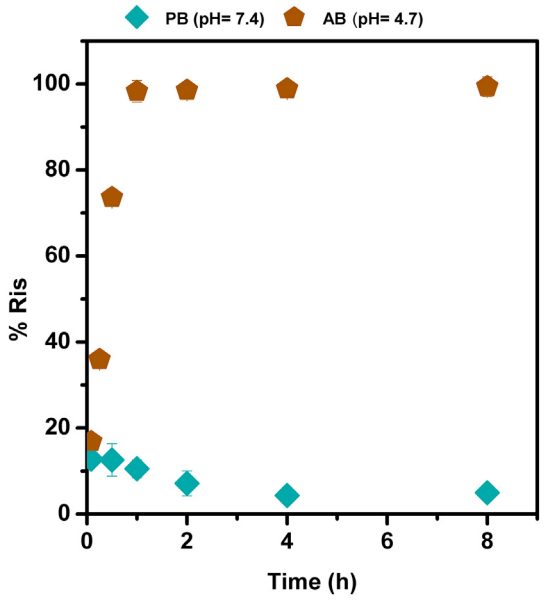

Fig. 4. Risedronate desorption (%Ris) kinetics from Ris functionalized LDH-NPs (1 g L^{-1}) dispersed in phosphate (PB) and acetate (AB) buffer solutions. Error bars represent the standard deviation, calculated from 3 experimental runs.

3.4. pH response of Ris functionalized LDH-NPs

pH responsive nanocarriers are particularly interesting for tumor targeting due to the acidic tumor microenvironment in solid tumors (Lee et al., 2008). Ris functionalized LDH-NPs showed significant changes in the physicochemical properties of functionalized LDH-NPs at the pH range between 9 and 5 (Fig. 5). In this pH range, only a slight proton uptake (Γ_H) and %Ris was measured while ζ increased up to a value similar to that of bare LDH-NPs, the iep being located at pH around 7. Accordingly, the aggregation of Ris functionalized LDH-NPs increased up to pH 7and diminished when ζ converged to that of bare LDH-NPs. The pH sensitivity of the functionalized LDH-NPs was related to the acid-base equilibria of Ris (Fig. 2A) which turned the trivalent $HRis^{3-}$ anion into the monovalent H_3Ris^{-} zwitter-ionrendering more positive the functionalized LDH-NPs.

Once the ζ was reversed, %Ris increased from <17% at pH = 6.3 to 67% at pH = 4.3. This is due to the lower affinity of H_3Ris^{-} zwitterions for LDH-NPs as well as the dissolution of the layers at pH < 5 (Parello et al., 2010). The dissolution process was also responsible of the steep Γ_H increase produced for both types of LDH-NPs in the 4–5 pH range. This process has been described as the main drug release mechanism from LDH nanocarriers and a route to render Ris functionalized LDH-NPs as a pH responsive material. Such a property is crucial when delivering pH sensitive drugs, such as etoposide (Zhu et al., 2016), to acidic organelles (late endosomes, lysosomes and mitochondria).

3.5. Hydroxyapatite binding capacity of Ris functionalized LDH-NPs

Although the pH responsiveness of Ris functionalized LDH-NPs is promissory for drug targeting to cancer cells, the main purpose of this functionalization was to produce osteotropicity. This capability was evaluated in vitro (Fig. 6), studying the interaction of Ris functionalized LDH-NPs with Ca^{2+} ions both in solution or at the surface of hydroxiapatite (Hap). First, the strong affinity for Ca^{2+} ions was evident from the %Ris, d and ζ determinations (Fig. 6A and B) which indicated the incorporation of this cation due to the chelation by $HRis^{3-}$ anions at the surface of the functionalized LDH-NPs. The incorporated Ca^{2+} improved the stability of the functionalization as well as compensated the negative charge of the Ris functionalized LDH-NPs with the consequent particle aggregation. This affinity was also responsible for the poor colloidal stability of Ris functionalized LDH-NPs in Ringer solution (Fig. 3).

The strong affinity of Ris functionalized LDH-NPs to Ca^{2+} ions was also responsible for the Hap binding capacity, which was tested by streaming potential measurements (Fig. 6C). As described in the literature (Knowles et al., 2000; Fahami et al., 2016), the ζ of Hap was negative and it became more positive (from −73 to −34 mV), when a stream of bare LDH-NPs was passed through Hap. On the contrary, when a dispersion of Ris functionalized LDH-NPs was passed on the same Hap sample, ζ turned to −132 mV. Clearly, Hap and bare LDH-NPs interacted by electrostatic interactions whereas Hap and Ris functionalized LDH-NPs presented the same negative charges. Consequently, in this case the measured ζ change was due to specific interactions between adsorbed $HRis^{3-}$ anions on LDH-NPs and Ca^{2+} ions at the surface of Hap. According to the literature, Ris anions strongly adsorb on Hap by ligand exchange reactions with surface phosphate anions (Al-Kattan et al., 2010; Errassifi et al., 2014). The adsorption mode is mainly through one of their phosphonate groups (Pascaud et al., 2013; Errassifi et al., 2014) although it has been proposed that binding by both phosphonate groups can be produced to a lesser extent. The interaction of Ris functionalized LDH-NPs with Hap might be then produced by $HRis^{3-}$ anions bridging where one of the phosphonate groups

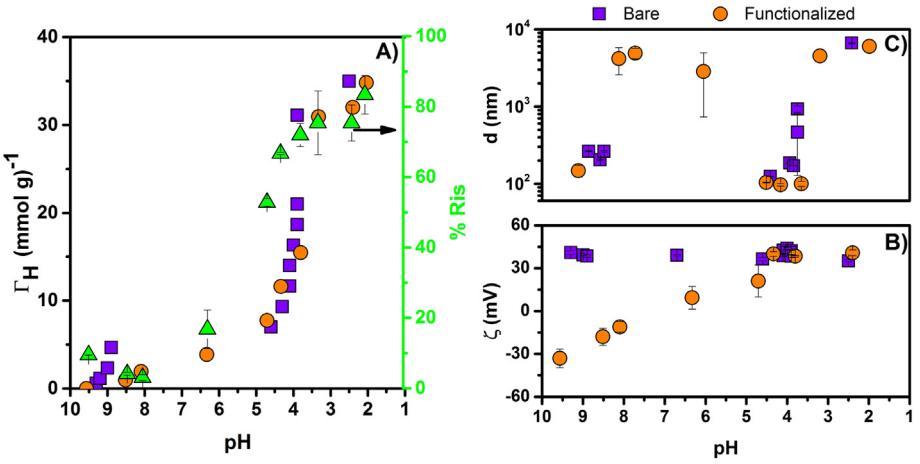

Fig. 5. A) Proton uptake (Γ_H) and Risedronate desorption (%Ris, triangles), B) hydrodynamic apparent diameter (d) and C) zeta potential (ζ) vs. pH curves for bare and Ris functionalized LDH-NPs. Error bars represent the standard deviation, calculated from 3 experimental runs.

interacted with Hap surface and the other one interacted with the LDH NP surface. The binding capacity of bare and functionalized LDH-NPs to Hap was also illustrated by SEM images of Hap disks before and after dipping in both dispersions (Fig. 6D). Hap showed globular particles that were irregularly disposed. On the other hand, the HAP surface was covered with planar, symmetrical particles upon dipping in either bare and Ris functionalized LDH-NPs.

4. Conclusions

LDH-NPs were functionalized with Ris, a bisphosphonate with affinity for hydroxyapatite and rich acid-base reactivity. At low concentrations, the trivalent $HRis^{3-}$ was incorporated preferentially to the LDH-NPs surface with high affinity, providing with a negative zeta potential that controlled the size at around 100 nm. Ris intercalation between the layers took place at higher concentration when LDH-NPs surface became saturated. As a consequence, Ris functionalized LDH-NPs with a minimum intercalation can be prepared, which will allow the incorporation of a pharmaceutically active anions between the layers.

The size of Ris functionalized LDH-NPs was not affected by the high ionic strength or the presence of proteins in simulated biological media. Further, the functionalization was stable against protein adsorption and anionic exchange but a pH diminution which turned the trivalent anion into a single charged one, removed the functionalization. As expected, Ris functionalized LDH-NPs were bioresponsive with a high sensitivity for pH changes and specific affinity for hydroxyapatite. Due to their

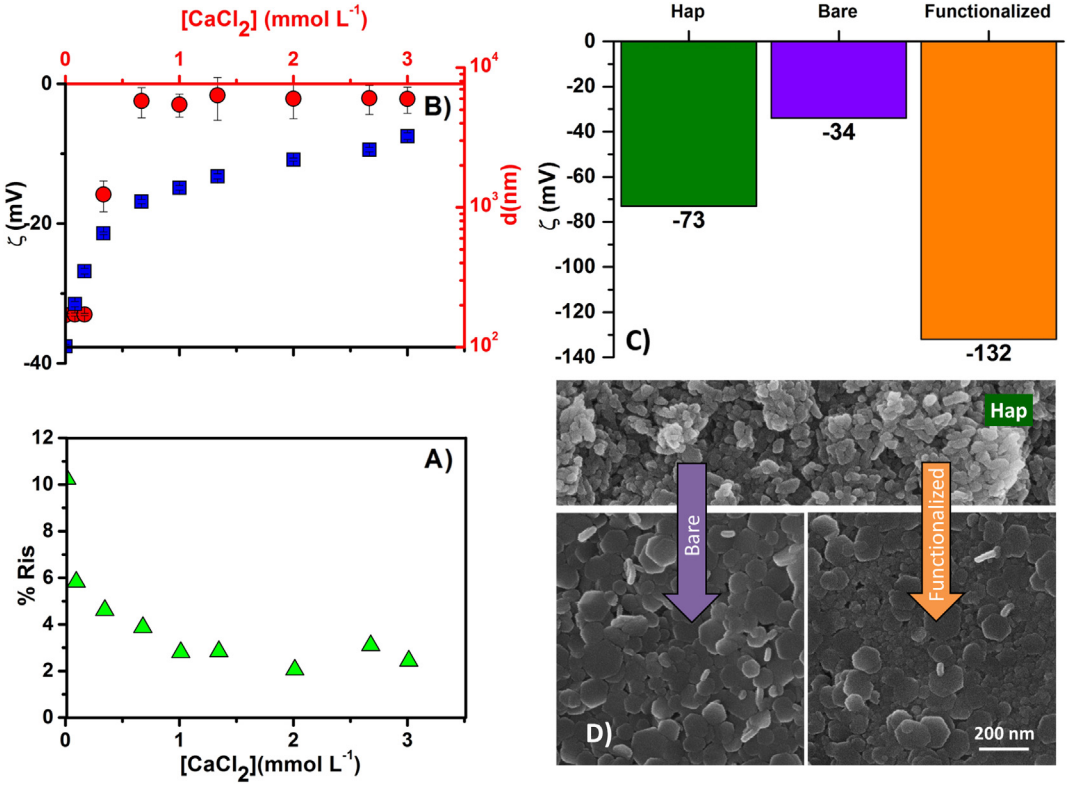

Fig. 6. A) Risedronate desorption (%Ris), B) zeta potential (ζ, squares) and hydrodynamic apparent diameter (d, circles) vs. $CaCl_2$ concentration ([$CaCl_2$]) curves for Ris functionalized LDH-NPs, C) zeta potential of hydroxyapatite (Hap) in 0.5 mmol L^{-1}KCl, bare LDH-NPs and Ris functionalized LDH-NPs dispersions (1 g L^{-1}, 0.5 mmol L^{-1}KCl), measured by streaming potential; D) SEM images of Hap before and after dipping in bare and functionalized LDH-NPs dispersions. Error bars represent the standard deviation, calculated from 3 experimental runs.

pH sensitive behavior and mostly, to their osteotropic capabilities, Ris functionalized LDH-NPs seem to be a promising alternative to produce LDH-based nanocarriers for bone therapies.

Acknowledgements

Economic supports by SeCyT-UNC, project number 05/C585, FONCyT, project PICT 12/0634, and CONICET, PIP 11220120100575, are gratefully acknowledged. CV and DAB acknowledge fellowships of ANPCyT and CONICET. The SEM images were obtained at the Laboratorio de Microscopía Electrónica y Análisis por Rayos X (LAMARX) and the Raman spectra at the Laboratorio de Nanoscopía y Nanofotónica, INFIQC-CONICET/UNC, Servicio Nacional de Microscopía – MINCyT.

Appendix A. Supplementary data

Supplementary data associated with this article can be found in the online version, at http://dx.doi.org/10.1016/j.clay.2017.03.001.

References

Al-Kattan, A., Errassifi, F., Sautereau, A.M., Sarda, S., Dufour, P., Barroug, A., Santos, I. Dos, Combes, C., Grossin, D., Rey, C., Drouet, C., 2010. Medical potentialities of biomimetic apatites through adsorption, ionic substitution, and mineral/organic associations: three illustrative examples. Adv. Eng. Mater. 12:224–233. http://dx.doi.org/10.1002/adem.200980084.

Chakraborti, M., Jackson, J.K., Plackett, D., Brunette, D.M., Burt, H.M., 2011. Drug intercalation in layered double hydroxide clay: application in the development of a nanocomposite film for guided tissue regeneration. Int. J. Pharm. 416:305–313. http://dx.doi.org/10.1016/j.ijpharm.2011.06.016.

Chen, M., Cooper, H.M., Zhou, J.Z., Bartlett, P.F., Xu, Z.P., 2013. Reduction in the size of layered double hydroxide nanoparticles enhances the efficiency of siRNA delivery. J. Colloid Interface Sci. 390:275–281. http://dx.doi.org/10.1016/j.jcis.2012.09.033.

Choi, S.-J., Choy, J.-H., 2011. Layered double hydroxide nanoparticles as target-specific delivery carriers: uptake mechanism and toxicity. Nanomedicine (Lond.) 6:803–814. http://dx.doi.org/10.2217/nnm.11.86.

Chung, H.-E., Park, D.-H., Choy, J.-H., Choi, S.-J., 2012. Intracellular trafficking pathway of layered double hydroxide nanoparticles in human cells: size-dependent cellular delivery. Appl. Clay Sci. 65–66:24–30. http://dx.doi.org/10.1016/j.clay.2012.06.007.

Coleman, R.E., McCloskey, E.V., 2011. Bisphosphonates in oncology. Bone 49:71–76. http://dx.doi.org/10.1016/j.bone.2011.02.003.

Conde, J., Dias, J.T., Grazú, V., Moros, M., Baptista, P.V., de la Fuente, J.M., 2014. Revisiting 30 years of biofunctionalization and surface chemistry of inorganic nanoparticles for nanomedicine. Front. Chem. 2:48. http://dx.doi.org/10.3389/fchem.2014.00048.

Conterosito, E., Croce, G., Palin, L., Pagano, C., Perioli, L., Viterbo, D., Boccaleri, E., Paul, G., Milanesio, M., 2013. Structural characterization and thermal and chemical stability of bioactive molecule–hydrotalcite (LDH) nanocomposites. Phys. Chem. Chem. Phys. 15:13418. http://dx.doi.org/10.1039/c3cp51235e.

Costantino, U., Bugatti, V., Gorrasi, G., Montanari, F., Nocchetti, M., Tammaro, L., Vittoria, V., 2009. New polymeric composites based on poly(-caprolactone) and layered double hydroxides containing antimicrobial species. ACS Appl. Mater. Interfaces 1: 668–677. http://dx.doi.org/10.1021/am8001988.

Errassifi, F., Sarda, S., Barroug, A., Legrouri, A., Sfihi, H., Rey, C., 2014. Infrared, Raman and NMR investigations of risedronate adsorption on nanocrystalline apatites. J. Colloid Interface Sci. 420:101–111. http://dx.doi.org/10.1016/j.jcis.2014.01.017.

Fahami, A., Beall, G.W., Betancourt, T., 2016. Synthesis, bioactivity and zeta potential investigations of chlorine and fluorine substituted hydroxyapatite. Mater. Sci. Eng. C Mater. Biol. Appl. 59:78–85. http://dx.doi.org/10.1016/j.msec.2015.10.002.

Gu, Z., Zuo, H., Li, L., Wu, A., Xu, Z.P., 2015. Pre-coating layered double hydroxide nanoparticles with albumin to improve colloidal stability and cellular uptake. J. Mater. Chem. B 3:3331–3339. http://dx.doi.org/10.1039/C5TB00248F.

Hu, H., Xiu, K.M., Xu, S.L., Yang, W.T., Xu, F.J., 2013. Functionalized layered double hydroxide nanoparticles conjugated with disulfide-linked polycation brushes for advanced gene delivery. Bioconjug. Chem. 24:968–978. http://dx.doi.org/10.1021/bc300683y.

Kankala, R.K., Tsai, P.-Y., Kuthati, Y., Wei, P.-R., Liu, C.-L., Lee, C.-H., 2017. Overcoming multidrug resistance through co-delivery of ROS-generating nano-machinery in cancer therapeutics. J. Mater. Chem. B 5:1507–1517. http://dx.doi.org/10.1039/C6TB03146C.

Knowles, J.C., Callcut, S., Georgiou, G., 2000. Characterisation of the rheological properties and zeta potential of a range of hydroxyapatite powders. Biomaterials 21:1387–1392. http://dx.doi.org/10.1016/S0142-9612(00)00032-6.

Kuo, Y.-M., Kuthati, Y., Kankala, R.K., Wei, P.-R., Weng, C.-F., Liu, C.-L., Sung, P.-J., Mou, C.-Y., Lee, C.-H., 2015. Layered double hydroxide nanoparticles to enhance organ-specific targeting and the anti-proliferative effect of cisplatin. J. Mater. Chem. B 3: 3447–3458. http://dx.doi.org/10.1039/C4TB01989J.

Kuthati, Y., Kankala, R.K., Lee, C., 2015. Layered double hydroxide nanoparticles for biomedical applications: current status and recent prospects. Appl. Clay Sci. 112–113: 100–116. http://dx.doi.org/10.1016/j.clay.2015.04.018.

Ladewig, K., Niebert, M., Xu, Z.P., Gray, P.P., Lu, G.Q.M., 2010. Efficient siRNA delivery to mammalian cells using layered double hydroxide nanoparticles. Biomaterials 31: 1821–1829. http://dx.doi.org/10.1016/j.biomaterials.2009.10.058.

Lee, E.S., Gao, Z., Bae, Y.H., 2008. Recent progress in tumor pH targeting nanotechnology. J. Control. Release 132:164–170. http://dx.doi.org/10.1016/j.jconrel.2008.05.003.

LeVasseur, N., Clemons, M., Hutton, B., Shorr, R., Jacobs, C., 2016. Bone-targeted therapy use in patients with bone metastases from lung cancer: a systematic review of randomized controlled trials. Cancer Treat. Rev. 50:183–193. http://dx.doi.org/10.1016/j.ctrv.2016.09.013.

Li, D., Xu, X., Xu, J., Hou, W., 2011. Poly(ethylene glycol) haired layered double hydroxides as biocompatible nanovehicles: morphology and dispersity study. Colloids Surf. A 384:585–591. http://dx.doi.org/10.1016/j.colsurfa.2011.05.012.

Ma, R., Wang, Z., Yan, L., Zhu, G., 2014. Novel Pt-loaded layered double hydroxide nanoparticles for efficient and cancer-cell speci fi c delivery of a cisplatin prodrug. J. Mater. Chem. B 2:4868–4875. http://dx.doi.org/10.1039/c4tb00645c.

Medina-Kauwe, L.K., Xie, J., Hamm-Alvarez, S., 2005. Intracellular trafficking of nonviral vectors. Gene Ther. 12:1734–1751. http://dx.doi.org/10.1038/sj.gt.3302592.

Meloun, M., Ferenčíková, Z., Málková, H., Pekárek, T., 2012. Thermodynamic dissociation constants of risedronate using spectrophotometric and potentiometric pH-titration. Cent. Eur. J. Chem. 10:338–353. http://dx.doi.org/10.2478/s11532-011-0150-3.

Nakayama, H., Takeshita, K., Tsuhako, M., 2003. Preparation of 1-Hydroxyethylidene-1,1-Diphosphonic Acid-Intercalated Layered Double Hydroxide and its Physicochemical Properties. 92 pp. 2419–2426.

Oh, J.-M., Choi, S.-J., Kim, S.-T., Choy, J.-H., 2006. Cellular uptake mechanism of an inorganic nanovehicle and its drug conjugates: enhanced efficacy due to clathrin-mediated endocytosis. Bioconjug. Chem. 17:1411–1417. http://dx.doi.org/10.1021/bc0601323.

Oh, J.-M., Choi, S.-J., Lee, G.-E., Han, S.-H., Choy, J.-H., 2009. Inorganic drug-delivery nanovehicle conjugated with cancer-cell-specific ligand. Adv. Funct. Mater. 19: 1617–1624. http://dx.doi.org/10.1002/adfm.200801127.

Ossipov, D.A., 2015. Bisphosphonate-modified biomaterials for drug delivery and bone tissue engineering. Expert Opin. Drug Deliv.:1–16 http://dx.doi.org/10.1517/17425247.2015.1021679.

Parello, M.L., Rojas, R., Giacomelli, C.E., 2010. Dissolution kinetics and mechanism of Mg-Al layered double hydroxides: a simple approach to describe drug release in acid media. J. Colloid Interface Sci. 351:134–139. http://dx.doi.org/10.1016/j.jcis.2010.07.053.

Pascaud, P., Gras, P., Coppel, Y., Rey, C., Sarda, S., 2013. Interaction between a bisphosphonate, tiludronate, and biomimetic nanocrystalline apatites. Langmuir 29:2224–2232. http://dx.doi.org/10.1021/la3046548.

Ramanlal Chaudhari, K., Kumar, A., Megraj Khandelwal, V.K., Ukawala, M., Manjappa, A.S., Mishra, A.K., Monkkonen, J., Ramachandra Murthy, R.S., 2012. Bone metastasis targeting: a novel approach to reach bone using Zoledronate anchored PLGA nanoparticle as carrier system loaded with Docetaxel. J. Control. Release 158:470–478. http://dx.doi.org/10.1016/j.jconrel.2011.11.020.

Ray, S., Joy, M., Sa, B., Ghosh, S., Chakraborty, J., 2015. pH dependent chemical stability and release of methotrexate from a novel nanoceramic carrier. RSC Adv. 5:39482–39494. http://dx.doi.org/10.1039/C5RA03546E.

Redman-Furey, N., Dicks, M., Bigalow-Kern, A., Cambron, R.T., Lubey, G., Lester, C., Vaughn, D., 2005. Structural and analytical characterization of three hydrates and an anhydrate form of risedronate. J. Pharm. Sci. 94:893–911. http://dx.doi.org/10.1002/jps.20308.

Rives, V., del Arco, M., Martín, C., 2014. Intercalation of drugs in layered double hydroxides and their controlled release: a review. Appl. Clay Sci. 88–89:239–269. http://dx.doi.org/10.1016/j.clay.2013.12.002.

Rodrigues, L.A.D.S., Figueiras, A., Veiga, F., de Freitas, R.M., Nunes, L.C.C., da Silva Filho, E.C., da Silva Leite, C.M., 2013. The systems containing clays and clay minerals from modified drug release: a review. Colloids Surf. B: Biointerfaces 103:642–651. http://dx.doi.org/10.1016/j.colsurfb.2012.10.068.

Rojas, R., Palena, M.C., Jimenez-Kairuz, A.F., Manzo, R.H., Giacomelli, C.E., 2012. Modeling drug release from a layered double hydroxide–ibuprofen complex. Appl. Clay Sci. 62–63:15–20. http://dx.doi.org/10.1016/j.clay.2012.04.004.

Saha, S., Ray, S., Acharya, R., Kumar, T., Chakraborty, J., 2017. Applied clay science magnesium, zinc and calcium aluminium layered double hydroxide-drug nanohybrids: a comprehensive study. Appl. Clay Sci. 135:493–509. http://dx.doi.org/10.1016/j.clay.2016.09.030.

Tantra, R., Tompkins, J., Quincey, P., 2010. Characterisation of the de-agglomeration effects of bovine serum albumin on nanoparticles in aqueous suspension. Colloids Surf. B: Biointerfaces 75:275–281. http://dx.doi.org/10.1016/j.colsurfb.2009.08.049.

Vasti, C., Bedoya, D.A., Rojas, R., Giacomelli, C.E., 2016. Effect of the protein corona on the colloidal stability and reactivity of LDH-based nanocarriers. J. Mater. Chem. B 4: 2008–2016. http://dx.doi.org/10.1039/C5TB02698A.

Vermonden, T., Giacomelli, C.E., Norde, W., 2002. Reversibility of structural rearrangements in bovine serum albumin during homomolecular exchange from AgI particles. Langmuir 17:3734–3740. http://dx.doi.org/10.1021/la010162o.

Wang, D., Miller, S.C., Kopecková, P., Kopecek, J., 2005. Bone-targeting macromolecular therapeutics. Adv. Drug Deliv. Rev. 57:1049–1076. http://dx.doi.org/10.1016/j.addr.2004.12.011.

Wang, L., Liu, Y., Li, W., Jiang, X., Ji, Y., Wu, X., Xu, L., Qiu, Y., Zhao, K., Wei, T., Li, Y., Zhao, Y., Chen, C., 2011. Selective targeting of gold nanorods at the mitochondria of cancer cells: implications for cancer therapy. Nano Lett. 11:772–780. http://dx.doi.org/10.1021/nl103992v.

Wang, X., Yang, Y., Jia, H., Jia, W., Miller, S., Bowman, B., Feng, J., Zhan, F., 2014. Peptide decoration of nanovehicles to achieve active targeting and pathology-responsive cellular uptake for bone metastasis chemotherapy. Biomater. Sci. 2:961. http://dx.doi.org/10.1039/c4bm00020j.

Wong, Y., Markham, K., Xu, Z.P., Chen, M., Max Lu, G.Q., Bartlett, P.F., Cooper, H.M., 2010. Efficient delivery of siRNA to cortical neurons using layered double hydroxide nanoparticles. Biomaterials 31:8770–8779. http://dx.doi.org/10.1016/j.biomaterials.2010.07.077.

Xu, Z.P., Stevenson, G., Lu, C.-Q., Lu, G.Q.M., 2006. Dispersion and size control of layered double hydroxide nanoparticles in aqueous solutions. J. Phys. Chem. B 110: 16923–16929. http://dx.doi.org/10.1021/jp062281o.

Zhang, X.-Q., Zeng, M.-G., Li, S.-P., Li, X.-D., 2014. Methotrexate intercalated layered double hydroxides with different particle sizes: structural study and controlled release properties. Colloids Surf. B: Biointerfaces 117C:98–106. http://dx.doi.org/10.1016/j.colsurfb.2014.02.018.

Zhu, R., Wang, Q., Zhu, Y., Wang, Z., Zhang, H., Wu, B., Wu, X., Wang, S., 2016. pH sensitive nano layered double hydroxides reduce the hematotoxicity and enhance the anticancer efficacy of etoposide on non-small cell lung cancer. Acta Biomater. 29:320–332. http://dx.doi.org/10.1016/j.actbio.2015.10.029.

Zuo, H., Gu, Z., Cooper, H., Xu, Z.P., 2015. Crosslinking to enhance colloidal stability and redispersity of layered double hydroxide nanoparticles. J. Colloid Interface Sci. 459: 10–16. http://dx.doi.org/10.1016/j.jcis.2015.07.063.